Current Environmental Health Reports (2025) 12:7
https://doi.org/10.1007/s40572-025-00473-y

REVIEW

Ways to Measure Metals: From ICP-MS to XRF

Kolawole E. Adesina[1] · Chandler J. Burgos[1] · Thomas R. Grier[1] · Abu S. M. Sayam[1] · Aaron J. Specht[1,2]

Accepted: 2 January 2025
© The Author(s), under exclusive licence to Springer Nature Switzerland AG 2025

Abstract

Purpose of Review This review explores the use of Inductively Coupled Plasma Mass Spectrometry (ICP-MS) and X-ray Fluorescence (XRF) for quantifying metals and metalloids in biological matrices such as hair, nails, blood, bone, and tissue. It provides a comprehensive overview of these methodologies, detailing their technological limitations, application scopes, and practical considerations for selection in both laboratory and field settings. By examining traditional and novel aspects of each method, this review aims to guide researchers and clinical practitioners in choosing the most suitable analytical tool based on their specific needs for sensitivity, precision, speed, and sample preparation.

Recent Findings Recent studies highlight enhanced capabilities of both ICP-MS and XRF technologies, making them more adaptable to various analytical needs. ICP-MS is renowned for its unmatched sensitivity and precision in detecting ultra-trace metals and metalloids in complex biological samples, such as lead in plasma or seawater. XRF advancements include lower detection limits and reduced sample preparation time, enabling rapid, non-destructive analyses, ideal for quick field assessments. Portable XRF analyzers have revolutionized on-the-spot testing, providing robust data without traditional wet-lab constraints. Moreover, hybrid techniques combining ICP-MS and XRF features are emerging, offering rapid and precise metal analysis for environmental monitoring, clinical diagnostics, and epidemiological studies.

Summary Matching analytical methods to specific research demands is critical. ICP-MS is the gold standard for detailed quantitative analysis in laboratories, while XRF excels in non-destructive, immediate field applications. Selection should consider sample complexity, sensitivity, speed, and cost-efficiency. Integrating ICP-MS and XRF offers a versatile approach to metals analysis, transforming practices in environmental science and healthcare diagnostics. As these technologies evolve, they are promising to expand capabilities in detecting and understanding the roles of metals and metalloids in health and the environment.

Keywords Metals · Quantification · XRF · ICP-MS · Biological samples · Elements · Spectrometry

Introduction

Quantifying trace metals is essential in various scientific fields [1]. While trace amounts of metals like calcium, manganese, and iron are crucial for human health, their excess or deficiency can cause health problems. Metals like cadmium, mercury, or lead are harmful even at trace levels. Previous literature has identified the significance of detecting, identifying, and evaluating trace metals across medical applications [2, 3], material sciences [4–6], and environmental studies [7–10].

A standard for metal measurements over the past two decades is inductively coupled plasma mass spectrometry (ICP-MS) [11, 12]. ICP-MS stands out for its exceptional sensitivity, broad dynamic detection range, and capability to analyze several metals at once across multiple biological matrices [13, 14]. ICP-MS has seen widespread use in quantifying elemental concentrations in a variety of biological samples including cells [15], hair and nails [16], lungs tissues [17], bio-fluids i.e., teardrops [18], urine [19], whole blood and plasma [20], and human serum [21, 22]. Over the years, several types of ICP-MS systems have been employed to analyze biological matrices with each one having its own advantages. Some of these enhanced ICP-MS used in measuring elemental contents includes quadrupole ICP-MS

✉ Aaron J. Specht
aspecht@purdue.edu

[1] School of Health Sciences, Purdue University, West-Lafayette, IN 47906, USA

[2] Harvard T.H. Chan School of Public Health, Boston, MA 02115, USA

Published online: 27 January 2025

(ICP-Q-MS) [23–26], high-resolution ICP-MS (HR-ICP-MS) [24, 27–35], triple quadrupole ICP-MS (ICP-MS/MS) [36–44], time-of-flight ICP-MS (TOF-ICP-MS) [45–50], and laser ablation ICP-MS (LA-ICP-MS) [51–61]. Selecting the right system involves assessing analytical needs like selectivity, throughput, and complexity of the biological matrix and elements involved.

X-ray fluorescence (XRF) is a non-destructive technique used for multi-elemental quantification. It uses an excitation source (e.g. X-ray tube) to excite electrons within a sample that upon deexcitation produce characteristic X-ray photons that is unique to each element. The intensities of the detected X-rays are proportional to the elemental concentrations present. This process does not alter the sample, and calibration methods simplify sample preparation. Some of the prevailing types of XRF suitable and adopted in biomedical research include energy dispersive XRF (EDXRF) [2, 51, 63–67], wavelength dispersive XRF (WD-XRF) [62, 68–70], micro-beam XRF (μ-XRF) [71–73], total reflection XRF (TRXRF) [74, 75], and synchrotron radiation XRF (SRXRF) [76–78]. Each use distinct methods for detecting and analyzing the fluorescent X-ray photons emitted by the specimen [73, 79]. Many of these XRF methods have been successfully applied to detect and measure metals in different biological samples including normal and cancerous tissues [80–82], hair [83–85], nails [83, 86–90], blood [2, 64, 66], and bones [78, 91–99].

This review compares different methods of metals quantification using ICP-MS and XRF to provide insights into current practices and suggest future directions for assessing biomarker exposure levels. It compares advantages and limitations between these methods in measuring metals regarding time, sample preparation, skill demands, and detection limits. Previous work has compared XRF to ICP-MS techniques in both instrumentation and the range of application [51, 100–102], but this review highlights the current trends in different modes and techniques of both instruments in a way to guide toxicological and environmental researchers in choosing the appropriate instrument for their needs evaluating the health impacts of metals.

Significance of Metals and Metalloids Quantification in Biological Systems

Trace metals are vital for health, however, deficiencies in ones like chromium, nickel, zinc, iron, or iodine lead to various conditions [103]. This underscores the need to detailed analysis of trace elements in medicine and clinical research. Analyzing bodily fluids and tissue samples is essential for health monitoring, and these biomonitoring efforts have used particular biomarkers like blood, nail, and bone to accomplish this [104]. These studies are primarily essential for health risk assessments and policy-making [105, 106] by tracking metal exposures across geographic locations [107], age groups [108], over activity periods [109], or even a combination of these factors [110]. Research into metal toxicity and related disorders is important due to the accumulation of metals and metalloid like arsenic, cadmium, chromium, mercury, and lead from contaminated sources. Analyzing biological specimens for trace minerals is essential due to their significant biomedical and pharmacological implications [111, 112].

Methodology of Study, Literature, and Search

To conduct our review of the assessment of trace metals in biological specimens using XRF and ICP-MS techniques, we employed the following approach. We used Google Scholar and PubMed with the following search terms: ("X-ray fluorescence" or "XRF") and ("inductively coupled plasma mass spectrometry" or "ICP-MS") and ("trace metals" or "metalloids") and ("biological specimens" or "biological samples") and ("quantification" or "detection"). We also found publications without Digital Object Identification from other sources like Research Gate. The search was limited to publications from 2015 to the present to capture recent advancements and current applications that use various biomarkers. Articles were screened based on their abstracts and titles, and those that met the inclusion criteria were subjected to a full-text review for detailed analysis. This methodology aimed to gather information on the performance, advantages, and limitations of XRF and ICP-MS for detecting and quantifying metals in health risk assessments, medical diagnostics, and environmental monitoring. This review aimed to identify knowledge gaps in trace element analysis and suggest future research directions.

Various Inductively Coupled Plasma-Mass Spectrometry Enhanced Techniques for Metal(loids) Analyses

This section details the operational principles, ionization methods, and mass detection systems of ICP-MS instruments and emphasizes their capabilities in analyzing trace metals analysis in various matrices.

Quadrupole ICP-MS (ICP-Q-MS)

Quadrupole Inductively Coupled Plasma Mass Spectrometry (ICP-Q-MS) combines the high-temperature capabilities of an ICP source with the precision of mass spectrometry to detect trace elements and some non-metals at very low concentrations. The technique involves converting a liquid

sample into a mist, ionizing it in an argon plasma, and analyzing the ions produced in a quadrupole mass analyzer based on their mass-to-charge ratios. ICP-MS offers high sensitivity to detect elements at the parts per trillion level and produces a wide spectrum of concentrations quickly in a single analysis run. However, it faces challenges from certain polyatomic ions and matrix effects that affect the results. Equipment costs range from $150,000 to $250,000 USD for entry level systems with ongoing expenses for high-purity argon gas and complex sample preparation. Additionally, ICP-MS requires skilled operators and regular maintenance to produce its accuracy. Despite these challenges, quadrupole ICP-MS is widely used in fields like geology, environmental science, and medicine [23, 113].

High-Resolution ICP-MS (HR-ICP-MS)

High-resolution Inductively Coupled Plasma Mass Spectrometry (HR-ICP-MS) enhances traditional ICP-MS capabilities by incorporating a magnetic sector or double focusing mass spectrometer to separate ions not only by their mass-to-charge ratio but also by energy. This separation significantly improves resolution that allows to distinguish analyte ions and interfering species of identical mass-to-charge ratios. HR-ICP-MS begins similarly to quadrupole ICP-MS but the ionized sample is passed through a magnetic sector field which separates ions based on their momentum. This addition minimizes but not completely removes spectral interferences, including those from polyatomic ions, which produces cleaner spectra and thus provides better trace element quantification.

HR-ICP-MS excels in sensitivity and specificity in being able to detect low-abundance isotopes and elements in complex matrices with minimal interference. It resolves isobaric and polyatomic interferences without chemical resolution, which is useful in fields like environmental monitoring and biomedical research. However, HR-ICP-MS systems are significantly more expensive than ICP-Q-MS with costs typically ranging from $400,000 to $600,000 USD. The instrument's complexity requires expertise in operation and maintenance, and its higher resolution results from longer analysis times compared to ICP-Q-MS, which reduces throughput. Despite these challenges, HR-ICP-MS has been highly effective in detecting and monitoring metals and nonmetals in biological fluids including blood plasma, blood spots, and tissues [27, 28, 30, 114].

Triple Quadrupole ICP-MS (ICP-QQQ-MS)

Triple Quadrupole ICP-MS (ICP-QQQ-MS) is a form of mass spectrometry that utilizes two quadrupole mass analyzers in series separated by a collision/reaction cell [115]. These systems allow for chemical collisions to prevent typical interferences seen in standard ICP-MS [14]. The use of collision-reaction-cells (CRC) and the implementation of a second scanning quadrupole in ICP-QQQ-MS stand out as pivotal developments that effectively eliminate spectroscopic interferences [116].

In ICP-QQQ-MS, the first quadrupole (Q1) selects precursor ions of a specific mass-to-charge ratio, which are then directed into the collision/reaction cell. Within this cell, ions can undergo reactions with a chosen gas, such as removing interferences or inducing predictable reaction products. The second quadrupole (Q2) analyzes the product ions at extremely low concentrations, often in the parts per trillion (ppt) or parts per quadrillion (ppq) range for some elements. By using reaction gases like ammonia or oxygen, ICP-QQQ-MS can break down or transform interfering species. This allows for the accurate quantification of target analytes by mitigating typical ICP-MS interferences like polyatomic or the plasma gas itself [117]. One of the standout features of ICP-QQQ-MS is its versatility in analyzing a wide range of biological samples, including blood, urine, tissue samples, and even complex environmental matrices. Its ability to provide precise and accurate measurements at trace levels makes it particularly valuable in environmental monitoring, clinical research, toxicology, and food safety testing.

With the average cost of an ICP-QQQ-MS system, like an Agilent 8900, typically ranging from $400,000 to $700,000 USD depending on the configuration and application requirements, the complexity of ICP-QQQ-MS systems requiring skilled operators to optimize the reaction cell conditions and interpret the more complex spectra, and having potentially longer analysis for reaction gas optimization, ICP-QQQ-MS has disadvantages for high-throughput or budget-constrained settings.

Time-of-Flight ICP-MS (TOF-ICP-MS)

Time-of-Flight Inductively Coupled Plasma Mass Spectrometry (TOF-ICP-MS) operates on the principle of ionizing sample constituents within a plasma source, accelerating their ions, and measuring their time of flight. This time is inversely proportional to the square root of the mass-to-charge ratio (m/z) and allows for the simultaneous detection of all present isotopes based on their distinct flight times to the detector in a single measurement [118]. This feature makes it particularly suitable for real-time, comprehensive elemental or isotopic overview like in environmental monitoring, food safety, forensic studies, and proteomics. This technique's high throughput and broad dynamic range facilitate the analysis of biological samples and plant materials, and it provides insight into trace elements and isotopic ratios. Unique to TOF-ICP-MS is its non-scanning operation mode which allows it to excel in applications where rapid, simultaneous multi-element detection is necessary, which

offers timesaving and efficiency improvements over other ICP-MS configurations.

With prices ranging from $500,000 to $800,000 USD and being more complex than traditional quadrupole or sector field ICP-MS systems, TOF-ICP-MS systems can be less accessible to labs. Additionally, careful calibration is needed as the broad mass range covered in each measurement can lead to variations in sensitivity across different elements and isotopes.

Laser Ablation ICP-MS (LA-ICP-MS)

Laser Ablation Inductively Coupled Plasma Mass Spectrometry (LA-ICP-MS) is an analytical technique that merges the direct solid sampling capability of laser ablation with the sensitivity and selectivity of ICP-MS for trace metal(loids) analysis [119]. It works by focusing a laser beam onto a sample surface to vaporize a minute area (micrograms of mass) that creates an aerosol that is then transported into an ICP-MS system for ionization and mass spectrometric analysis. This process allows for the rapid, in-situ analysis of solid samples with minimal preparation. One of the primary merits of LA-ICP-MS is its ability to perform spatially-resolved analyses to create detailed mapping of elemental distributions within solid biological matrices including human hair, organs, soft tissues, bone, teeth, and others [53, 55–57, 60], which offers insights into historical pollution levels or dietary habits.

LA-ICP-MS can be susceptible to matrix effects where the composition of the sample can influence the ablation process and, consequently, the analytical results. Calibration can also be complex, often requiring matrix-matched standards for accurate quantification. Furthermore, the initial cost and operational expertise required for LA-ICP-MS can be significant barriers to its widespread adoption with costs ranging from $400,000 to $700,000 USD.

Emerging X-ray Fluorescence Methodologies for Metals Analyses

This section reviews the most popular XRF spectrometers, their principal energy setups, function, and limitations and significant advantages, particularly in their application to biological systems [120]. Figure 1 illustrates some of the major instrumentation differences between these techniques.

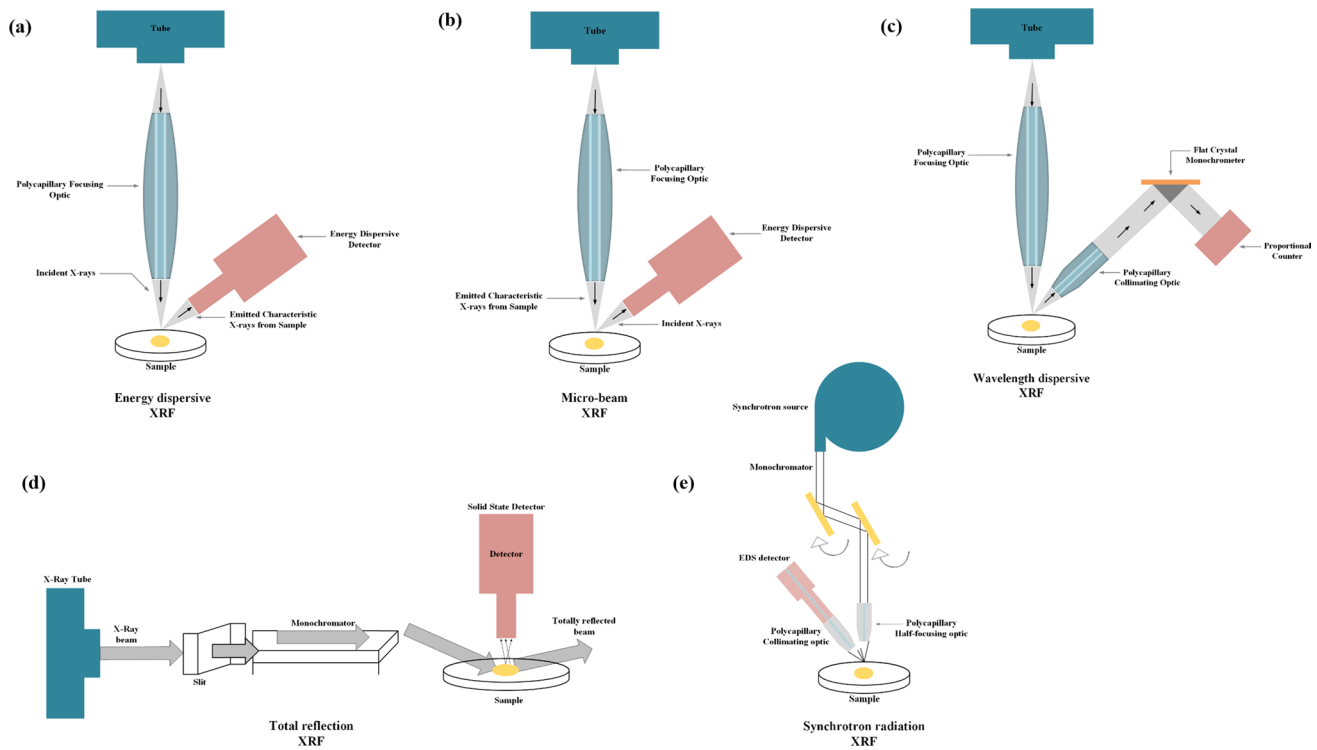

Fig. 1 XRF spectrometry configurations and geometries. (**a**) EDXRF (**b**) μ-XRF (**c**) WDXRF (**d**) TRXRF (**e**) SRXRF

Energy Dispersive XRF (EDXRF)

Energy Dispersive XRF (EDXRF) uses a detector to discern varying energy levels of characteristic radiation from the sample, creating an XRF spectrum by counting X-rays at each energy level. However, background noise from scattered radiation complicates the detection of low-intensity peaks, which creates some accuracy challenges in trace metal concentrations.

Elemental quantification in EDXRF identifies a sample's elemental makeup by evaluating X-ray fluorescence intensities from elemental peaks using comparative standards. EDXRF has multiple configurations for the x-ray anode, but all essentially act similarly [121, 122].

Most EDXRF devices can measure most elements accurately, but elements lighter than sodium yield poor results due to their low yield and absorption of photons by air. Lighter elements are better measured using a vacuum or with a helium purge and a specific light element detector. EDXRF is preferred for assessing lead levels in blood samples due to its minimal sample requirement, non-destructive nature, and adaptability. EDXRF spectrometers are compact, cost-effective (prices range from $50,000 to $200,000 USD), and straightforward, which make them a preferred choice over other analytical technologies [2, 64, 67].

Wavelength Dispersive XRF (WDXRF)

Wavelength Dispersive XRF (WDXRF) spectrometers utilize a crystal to separate various energy levels. All radiation emitted from the sample is directed onto the crystal, which then diffracts each energy at different angles [123].

Both EDXRF and WDXRF allow for the direct analysis of solid materials without damaging them. However, particularly for analyzing biological specimens, EDXRF is comparatively more suitable for its efficacy and practicality to WDXRF [124]. The initial setup of a WDXRF spectrometer shares features with the 2D optical and non-secondary EDXRF spectrometers, where the sample is exposed to radiation and is then detected [68, 69]. In WDXRF spectrometry, gas-filled and scintillation detectors are important components due to their effectiveness in detecting different ranges of X-ray energies since neither type is fully efficient across the entire energy spectrum of 1 to 20 keV. WDXRF spectrometers normally consist of a mix of these detectors, including gas-filled, scintillation, and sealed counters, to ensure a broad and effective detection range [70]. Another key distinction between the two methods is that EDXRF systems capture the entire spectrum almost instantly, allowing for the simultaneous determination of a wide array of elements. In contrast, WDXRF systems collect the spectrum through a sequential process. This method is not only more time-intensive but also incurs higher costs because of the limited number of detectors available [125]. Compared with the desktop versions of EDXRF, WDXRF systems can start around $100,000 up to $500,000 USD. These systems were routinely used in air filter analysis but have largely been replaced by smaller, more powerful EDXRF devices [126].

Micro-Beam XRF (μ-XRF)

The μ-XRF technique offers a non-destructive method to visualize high-resolution spatial information for each analyzed element [73]. In μ-XRF, the X-ray flux is collimated through an optical arrangement like a pinhole aperture or polycapillary optical system with a micrometer scale diameter and hits the samples. It then emits fluorescence radiation which the detector extracts the sample's elemental information from the absorbed characteristic X-rays. The projected X-ray beam in this system ranges from 10 μm to 0.1 nm depending on the focusing optics or pinhole used. μ-XRF can also provide 3D elemental profiling through sequential 2D measurements.

μ-XRF can use either synchrotron-based or laboratory-based X-ray production. Synchrotron radiation (SR) generates powerful emissions including ultraviolet, visible, and infrared light, producing radiation levels much higher than those found in typical laboratory X-ray sources, which allow for ultra-low detection limits. The synchrotron beamline essentially reduces the incoming X-rays to a semi-monoenergetic peak which drastically improves the signal-to-noise ratio in spectral counts [73, 127]. SR can assess a broad spectrum of elements in concentrations from 0.01 to 1,000,000 μg/g with high beam alignment accuracy and fine focus, making it ideal for microanalysis. It has been used for elemental profiling of dental, skin, breast, and brain tissues [128–130]. Despite these features, analysis is limited due to their availability and complexities. To resolve this issue, lab-based μ-XRF was developed to provide similar elemental profiling capabilities and fine resolution with different optical systems [73].

The key difference between the benchtop and synchrotron-based μ-XRF is in the spatial resolution and beam flux, which ultimately influences detection limits. Synchrotron facilities use collimators because of the high intensity beams, whereas benchtop systems require mono or polycapillary optical systems. Benchtop μ-XRF fine-tunes elemental detection through voltage adjustments and different filters [131] often employing a separate low-energy detector to detect lighter elements as low as carbon.

The benchtop μ-XRF system has already been applied to analyze a some organ tissues, but not to the same extent that synchrotron has been used [132]. As benchtop μ-XRF continues to develop, it promises to enhance biological and environmental toxicity analysis and exposure assessment by providing high-resolution and sensitive elemental

profiling using a lab-based setting. Meanwhile, synchrotron-based systems will continue to provide high precision and sensitivity for trace elemental analysis in biological samples.

Total Reflection XRF (TRXRF)

Total Reflection XRF (TRXRF) directs a monochromatic X-ray beam at an angle below the critical angle to minimize background scatter and enhance detection capabilities. The beam, focused through a slit, is directed unto the specimen support layer and optimally excites the sample [62, 133] This technique minimally penetrates the sample support, which significantly reduces background scatter and in turn enhances detection capabilities (ppb or less).

TRXRF has limits of detection (LODs) in the range of 0.1 to 10 ppb for many elements such as lead (Pb), cadmium (Cd), and mercury (Hg), and 10 to 100 ppt for certain elements like arsenic (As) and selenium (Se). However, TRXRF faces challenges related to sample preparation, often requiring dissolution which can damage the sample [134]. The samples typically need to be homogenized and applied to the measurement surface uniformly for unbiased results. While ICP-MS require several milliliters of solution, corresponding to milligrams of a biological sample, TRXRF can achieve comparable detection limits (ppb or even less) using only microliters of solution [135].

Matrix effect removal in TRXRF focuses on minimizing background noise [136]. Biological samples, often containing low-Z elements, can scatter X-rays intensively which affects detection limits. Careful sample preparation allows for direct analysis with TRXRF by requiring only microgram quantities of the sample for multi-element analysis at the same time [76]. This makes TRXRF suitable for low-mass or liquid biological samples [74]. Similarly to other XRF techniques, using light element detectors without windows and performing detection in a vacuum enables accurate measurement of lighter elements down to carbon accurately.

Analytical Features and Capabilities of XRF and ICPMS Devices

Recent advancements in XRF methodologies have increased detection capabilities, broadened the spectrum of analyzable sample types, and improved the excitation of electron shells. The X-ray source configuration played a critical role in this advancement, as illustrated in Fig. 1 [120]. Tables 1 and 2 compare the analytical attributes, merits, and demerits of various advanced XRF and ICPMS methodologies respectively.

Applying Spectrometry to Assess Metals in Biological Systems

ICP-MS and its variations are the benchmark for trace element analysis due to their sensitivity and, with sample preparation, homogeneity of measurement. However, advanced XRF technologies with improved detectors, excitation sources, and data processing now offer comparable results for many applications. XRF excels in non-destructiveness, minimal sample preparation, and direct solid sample analysis and offers rapid turnaround and sample preservation. Handheld XRF provides quick, non-destructive ppm-level results of bulk measurements whereas portable ICP-MS requires more preparation. For spatial distribution studies, both XRF and LA-ICP-MS are valid, where XRF offers stable calibrations and LA-ICP-MS provides more precise sampling areas. The choice between ICP-MS and XRF depends on study requirements like sensitivity, throughput, and sample integrity. Both techniques are indispensable for understanding metal dynamics in biological environments. Tables 3 and 4 highlight recent advancements and biological applications of XRF and ICP-MS in bio-assessing metals and metalloids in hair, nails, blood, and bone samples.

Merits and Limitations of Both Instruments

When choosing a quantification method for assessing metals exposures in biological matrices, both ICP-MS and XRF offer unique advantages and limitations. The decision between ICP-MS and XRF should be guided by the scientific, practical, and financial contexts of the research project. Several major factors that influence selection capabilities are highlighted below:

- **Sample integrity:** ICP-MS typically requires the sample to be dissolved in strong acids, a process that destroys the original form of the sample. Conversely, XRF offers a non-destructive approach [90].
- **Throughput and Speed:** ICP-MS requires extensive sample preparation, including digestion or dissolution with strong acids, which can be time-consuming and requires careful handling to avoid contamination. This preparation extends the time from sample collection to result. However, once prepared, it can quickly analyze samples in succession. XRF can deliver quicker individual sample analysis times due to minimal preparation requirements, which speed up the overall workflow in settings that demand rapid results [86, 140].
- **Benchtop vs. Portable Analyzers:** Reliance on sophisticated lab facilities and preparation means benchtop

Table 1 Comparison of analytical attribute with merits and demerits of different advances of XRF methodologies

Analytical Capabilities	EDXRF	WDXRF	SRXRF	TRXRF	μXRF
Excitation source	Radioisotopes or X-ray tubes	Radioisotopes or X-ray tubes	Synchrotron particle accelerator	High powered X-ray sources (scaled tubes or rotating anode)	Micro-focused X-ray tubes or polycapillary optics
Detectable elements	C (6) – U (92)	Be (4) – U (92)	B (5) – U (92)	C (6) – U (92)	C (6) – U (92)
Mapping/imaging enablement	No	No	Yes	No	Yes
Compton contribution	Present but greatly reduced	Present but greatly reduced	Present but greatly reduced	Present but greatly reduced	Minimal due to focused nature of beam
Detection capabilities	ppb to bulk	ppm to bulk	ppt to bulk	ppt to bulk	ppm
Calibration standards	Necessary	Necessary	Necessary	Single element liquid standards used as internal standards	Necessary
Typical analyte mass used	micrograms to a few grams	micrograms to grams	ng to milligram range	Around 5 to 100 µl	ng/cm^2 to mg/cm^2
Sample to detector distance	~0.5 – 5 mm	Few cm	Few mm	~25 – 40 mm	Few mm – 2 cm
Types of sample	Solids, liquids, powder, thin film	Solids, powders, liquids, and thin films (Mostly homogenous and flat for optimal results)	Solids, liquids, or gaseous samples, and thin films	Liquids, granular materials (Samples homogenized into liquid form typically)	Solids, thin films, powders, and even liquids (with suitable holders)
Techniques nature	Non-destructive	Non-destructive	Non-destructive	Destructive for non-liquid samples requiring preparation	Non-destructive
Matrix effects	Significantly reduced	Greatly reduced	Significantly reduced	Absent	Significantly reduced
Need for sample preparation	No	Yes (grinded, homogeneous, fused into beads, or pressed into pellets)	No	Yes (digestion and suspension)	No
Element limitations	Decreased sensitivity at $Z < 14$	Decreased sensitivity at $Z < 11$	$Z < 5$	Decreased sensitivity at $Z < 14$	Decreased sensitivity at $Z < 13$
Analysis time	Less than 3 min	Greater than 5 min	Varies with sample sizes	Less than 3 min	Varies with sample sizes

Table 2 Comparison of analytical attribute with merits and demerits of different advances of ICP-MS methodologies

Analytical Capabilities	ICP-Q-MS	HR-ICP-MS	LA-ICP-MS	TOF-ICP-MS	ICP-QQQ-MS
Excitation source	Plasma source	Plasma source	Laser to plasma source	Plasma source	Plasma source
Detectable elements	Li (3) – U (92)	Li (3) – U (92)	Al (13) – U (92)	Li (3) – U (92)	Li (3) – U (92)
Detection capabilities	ppt to ppm	ppt to bulk	ppm to bulk	ppt for specific elements to ppm	ppt for many elements to ppm
Mapping/imaging enablement	No	No (Unless coupled with LA)	Yes (Limited: ablated surface)	Yes (for some setups)	No
Typical analyte mass used	ng to µg range	ng to µg range	ng to µg range	ng to µg range	pg to µg range
Compton contribution	Not applicable	Not applicable	Not applicable	Not applicable	Not applicable
Need for sample preparation	requires dilution or digestion of solid samples into liquid	requires dilution or digestion of solid samples into liquid	Digestion not required	requires dilution or digestion of solid samples into liquid	requires dilution or digestion of solid samples into liquid
Calibration standards	Yes	Yes	Yes	Yes	Yes
Types of sample	Mostly used for liquids and digested environmental samples	Versatile in analyzing liquids, solids (via laser ablation), and gases	Metals, glasses, biological tissues, and geological specimens	Liquids, solids, powders, biological, and environmental samples	Liquids, solids require digestion, & biological tissues, environmental samples
Techniques nature	Destructive	Destructive	Semi-destructive	Destructive	Destructive
Matrix effects	Greatly reduced	Greatly reduced	Greatly reduced	Greatly reduced	Greatly reduced
Element limitations	$Z < 7$	$Z < 7$	$Z < 11$	$Z < 7$	$Z < 7$
Analysis time	Between 30 min to hours	Between 30 min to hours	Between 30 min to hours	Few minutes	Between 30 min to hours
Interference Reduction	Kinetic Energy Discrimination	High energy resolution discrimination	Kinetic Energy Discrimination (SQ) or Chemical Reactions (QQQ)	Mass discriminatory; identifying unknowns	Kinetic Energy Discrimination and chemical reaction gases
Specific remarks	quadrupole mass filter to separate ions based on their mass-to-charge ratio	Utilizes a high-resolution mass spectrometer	Unique sample introduction system that uses a laser to vaporize the sample material	ideal for high-throughput elemental analysis, excelling in speed	Quantifies elements removes polyatomic and isobaric interferences

Table 3 Selected recent applications of XRF in metals and metalloids assessment of biomarkers (hair, nail, blood, bone, and tissue)

Biological Samples	XRF Technique	Excitation Source	Specifications (Current, Voltage, and Energy)	Elements & Limit of Detection (LOD)	Measurement Time per Sample	Ref
Bone	Micro-EDXRF	X-ray tube with a molybdenum target	500 µA, 40 kV, and Si(Li) detector	Ca (288), P (6428), Fe (68), Zn (17), and Sr (20)—all in µg g^{-1}	20 s	[137]
Bone	KXRF & portable XRF	KXRF—Cd-109 & PXRF—X-ray tube	PXRF—40 µA, 50 kV; KXRF—high-purified germanium (HpGe) detectors	Pb (not specified)	PXRF—3 min	[99]
In-vivo (skin tissue)	Portable XRF	Pu-238 X-ray source	Si-PIN photodiode detector at 13 & 17 keV	Fe (13 µg g^{-1})	50 s	[138]
Blood and skin tissue	XRF system & Handheld XRF Analyzer	Molybdenum target X-ray tube	XRF system—40 kV; Handheld XRF Analyzer—15 kV Silicon drift detector at 17 keV	Fe (not specified)	Handheld XRF—300 s	[139]
Blood	Desktop XRF & Micro-XRF	Si semiconductor X-ray detector & W anode X-ray tube	Desktop XRF—1 mA, 50 kV; Micro-XRF—700 µA, 50 kV	Pb (2.4, 2.4, 1.7, 1.4)—all in ppm	15, 30, 45, 60 s	[140]
Condor bone	Handheld XRF	Bi-83 X-ray tube	Silicon drift detector	Al, Si, P, S, K, Ca, Ti, V, Cr, Mn, Fe, Zn, Ag, Cd, Sn, & Sb (not specified)	2 min	[141]
Condor bone	KXRF & portable XRF	KXRF—Cd-109 & PXRF—X-ray tube	PXRF—40 µA, 50 kV; KXRF—high-purified germanium (HpGe) detectors	Pb (not specified)	PXRF—3 min KXRF—30 min	[92]
Blood	Synchrotron Radiation XRF	Radiation	2.5 GeV with a current intensity of 150–250 mA & incident X-ray energy at 18 keV in Si (Li) solid state detector	Ca, Zn, & Ti (imaging)	5 s	[142]
Toenail	Portable XRF	X-ray tube	50 µA, 40 kVp, and thermo-electric-cooled silicon drift detector up to 50 keV with silver (Ag) and iron (Fe) combination filter	Mn (3.65) and Hg (0.55)—both in µg g^{-1} (ppm)	3 min	[87]
In-vivo toenail	Portable XRF device	X-ray tube settings	40 µA, 50 kV with a transmission-type silver anode, iron, and silver filter	Mn (2.6 µg/g) and Hg (0.5 µg/g)	3 min	[88]
Toenail clippings	EDXRF— Portable XRF	X-ray tube	40 µA, 50 kV with a transmission-type silver anode, iron, and silver filter	Mn (3.2 µg/g) and Pb (0.6 µg/g)	3 min	[143]
Human finger and toenail	Portable XRF	Miniature X-ray tube	20 µA, 40 kVp	As (not specified)	180 s	[144]

Table 3 (continued)

Biological Samples	XRF Technique	Excitation Source	Specifications (Current, Voltage, and Energy)	Elements & Limit of Detection (LOD)	Measurement Time per Sample	Ref
Human toenail clippings	Portable XRF device	Molybdenum X-ray tube	200 µA, 50 kV, molybdenum Kα X-ray at an energy of approx. 17.5 keV was adopted as excitation beam	Zn (1.6 µg/g)	900 s	[145]
Toenail clippings	HD-Mobile XRF(Benchtop mode)	Molybdenum X-ray tube	200 µA and a tube voltage ranging up to 50 kV with mono-energetic at 17.5 keV (molybdenum Kα), & Silicon drift detector	As (0.1 µg/g)	900 s	[146]
Human nail	Portable XRF system	Rhodium target X-ray tube	100 µA, 40 kV, silicon drift detector (SDD), and range of spectra energy of interest between 7.85 – 10.11 keV	Zn (0.15 ± 0.01 ppm—open beam and 1.13 ± 0.08 ppm—weld mask)	120 s	[147]
Single nail clipping	HD-Mobile portable XRF	Molybdenum target X-ray tube	mono-energetic beam—17.4 keV (molybdenum Kα) with energy spectra analysis ranging from 10–13 keV	As and Se (both ≤ 0.3 µg/g)	3 min	[148]
Nail and hair	HD-Mobile XRF (Benchtop mode)	Molybdenum X-ray tube	200 µA and a tube voltage ranging up to 50 kV with mono-energetic at 17.5 keV (molybdenum Kα), and silicon drift detector	Zn (not specified)	300 s	[149]
Human toenail	Portable XRF device	X-ray tube	40 µA, 50 kV, and Si radiation detector using a silver filter	Ni (3.53), Zn (2.87), As (1.27), Se (4.60), and Pb (0.58)—all in mg/kg	3 min	[86]
Carpal and tarsal bones	EDXRF device	X-ray tube	Two Energy Dispersive XRF silicon drift detectors of 15 & 20 kV	P to Pb (not specified)	1 min per operating voltage	[150]
Human tibiae bone	KXRF system	Am-241 excitation source	HPGe detector peak at 0.67 keV	La (0.4 µg g^{-1}) and Gd (0.5 µg g^{-1}) bone minerals	30 min	[151]
Avian bone	Portable XRF device	X-ray tube	40 µA, 50 kV, and Si radiation detector using a silver and iron filter	Pb (not specified)	3 min	[152]
Repository skeletal bone	Portable XRF device	X-ray tube	40 µA, 50 kV, and Si radiation detector using a silver and iron filter	Pb (2.1 ± 0.5 µg g^{-1})	3 min	[153]
Liver tissues	Confocal micro-beam µ-XRF	Microfocus X-ray source with a molybdenum target	0.5 mA and 20 kV and a focal size of 16.5 µm corresponding half lens was connected to a silicon PIN detector	K, Fe, and Zn (imaging)	300 s	[154]

Table 3 (continued)

Biological Samples	XRF Technique	Excitation Source	Specifications (Current, Voltage, and Energy)	Elements & Limit of Detection (LOD)	Measurement Time per Sample	Ref
Human cortical bone tissue	Submicro- and micro- XRF (SR-XRF)	Diamond light source	W-Si multilayer monochromator, 2 polycapillary half-lenses, a 20 µm Al filter detector, Vortex 50 mm^2 silicon-drift detector, and XIA Mercury digital pulse processor	Ca, Zn, and Gd (imaging)	15 – 20 s per spot (pixel)	[155]
Distant tissues	Synchrotron radiation XRF	UVX Light source polychromatic beam	X-ray beam to a precise spot size of 20 µm, resolution of 140 eV at 5.9 keV, and a silicon drift detector	P, S, K, Ca, Mn, Fe, Cu, and Zn (imaging)	Not specified	[156]
Human hair	EDXRF	X-ray tube	X-ray emitted radiation range to samples were at 20 – 30 eV, 30 – 40 mA per sec	Na, Mg, Al, Si, P, S, Cl, K, Ca, Ti, Cr, Mn, Fe, Ni, Cu, and Zn (not specified)	40 min	[157]
Mouse brain tissues	Synchrotron µ-XRF	Maia XRF detector system	Double crystal monochromatic at 18 keV at optimized of Pb L-XRF focused to 1×0.6 μm^2 using Rh coated Kirkpatrick-Baez (KB) mirror optic producing flux in focused beam of $\sim 2 \times 10^{10}$ photons/s	Pb and Se (imaging)	dwell time for mic brain ranged between 100 – 150 ms/ per scan point	[158]

Table 4 Selected recent applications of ICPMS in metals and metalloids assessment of biomarkers (hair, nail, blood, bone, and tissue)

Biological Samples	ICP-MS Technique	Elements & Limit of detection (LOD)	Preparation & Matrix/ Background	Ref
Human toenail	ICP-MS	Ni (2.90), Zn (10.1), As (0.181), Se (0.994), and Pb (0.670)—all measured at ppb	Robust plasma and ultrahigh matrix introduction (UHMI), samples digested in nitric acid (0.001%) at 100 ℃ for 1 h, then cooled and diluted to 10 mL with type 1 water	[86]
Hair and nail	ICP-MS	Al (10 & 10), Ti (5 & 10), V (5 & 5), Cr (5 & 0.5), Mn (5 & 0.5), Fe (10 & 10), Co (0.1 & 0.1), Ni (5 & 0.5), Cu (5 & 4), Zn (8 & 8), Cd (0.05 & 0.05), & Pb (0.0 & 0.01)—hair & nail respectively all measured in mg kg^{-1}	65% nitric acid (HNO_3), 30% hydrogen peroxide (H_2O_2), and 30% hydrochloric acid (HCl) transferred to 25-mL of ultrapure water	[159]
Cortical bone	ICP-MS	Gd (0.8 ng/g) in bone	Each 0.5 g and roughly a quarter to one-third of the total bone length were homogenized and mixed with 50 µL of 100 nM $Tb(NO_3)_3$ as an internal standard. Dried for 2 h at 95 °C & were treated with 50 µL of 65% nitric acid and 20 µL of hydrogen peroxide (H_2O_2) then heated in a microwave at the same temperature for tissue dissolution	[160]
Fish tissues and organs	ICP-MS	Al (0.03), As (0.004), Cd (0.001), Co (0.003), Cr (0.04), Cu (0.01), Ni (0.005), Pb (0.002), and Zn (0.01)—all in µg/g	0.25 g of roach and silver bream, and 1.00 g of crucian carp were treated with 3 mL and 9 mL of 65% nitric acid respectively, along with 0.5 mL of 30% hydrogen peroxide. Then microwaved in an Ethos One at 1500 W, ramping to 200 °C over 15 min and holding for 45 min. The samples were transferred into 10 mL volumetric flasks and topped up with deionized water to volume	[161]
Tissues	ICP-MS	Al (0.5), Ca (1.2), Fe (0.2), K (4.1), Mg (0.3), Na (0.11), P (1.3)—measured at ppb; and As (1.1), Ba (6.8), Cd (5.2), Co (2.1), Cr (11), Cu (6.3), Hg (0.5), Mn (35), Mo (19), Ni (6.3), Pb (1.9), Rb (5.6), Sb (1.3), Sn (10), Sr (3.7), Te (4.8), Ti (5.6), Tl (0.1), V (2.4), Zn (6.3)—measured at ppt	Sheep tissue and bone samples, each weighing approximately 100 mg, along with blood samples ranging from 0.2 to 2.0 ml, were placed in a digestion vessel and digested with 8.0 ml of 67–69% HNO_3 using the Animal Tissue method. Post-digestion, these samples were diluted to a total volume of 20 ml using de-ionized water	[162]
Toenails	LA-ICP-MS	As (0.03 µg/g)	After rinsing twice with Milli-Q water, the samples were dried at 60 °C for 1–2 days, ground, and weighed for digestion in nitric acid using a controlled block digestion system. The digestion process involved gradual heating to 100 °C, addition of hydrogen peroxide, and further heating at 95 °C. Samples were finally diluted to 10 ml with deionized water, vortexed, and analyzed for total metal content	[163]
Human hair and nail	ICP-MS	As, Cd, Cu, Pb, Zn, Mn, Co, Mo, and Ba (not specified)	Samples were placed in vessels and treated with 8 ml of nitric acid before heating. To maintain cleanliness and avoid contamination, all vessels were soaked in a 20% nitric acid solution for 24 h, rinsed three times with Milli-Q water, and reused. After digestion, samples were diluted at a 1:20 ratio with Milli-Q water to avoid techniques saturation	[164]

Table 4 (continued)

Biological Samples	ICP-MS Technique	Elements & Limit of detection (LOD)	Preparation & Matrix/ Background	Ref
Nail clippings	ICP-QQQ-MS	Hg, As, Cd, Co, Cr, Cu, Fe, Mn, Pb, and Se (not specified)	Nails were cleared of any visible contaminants and submerged in acetone within a polyethylene vial for a 20-min ultrasonic bath. Subsequent cleansing involved a 1% Triton X-100 solution followed by several deionized water rinses, effectively removing external impurities without leaching internal metal content. Then subjected to acid digestion using HNO_3 in a MARS6 microwave digestion unit, tailored to each sample's weight	[165]
Toenails	ICP-MS	V, Cr, Mn, Fe, Co, Ni, Cu, Zn, Ga, As, Se, Rb, Sr, Cd, Tl, Pb, Th, and U (not specified)	A 50 µg/L scandium internal standard in 1% nitric acid was incorporated to ensure accuracy, and kinetic energy mode was employed for all metals except selenium, which was analyzed in standard mode. High purity helium was utilized as a collision gas to enhance detection sensitivity. Calibration standards ranged from 0.01 to 100 µg/L across a nine-point curve to ensure robust quantification, with quality control checks at 1 and 10 µg/L conducted after every 15 samples	[166]
Hair, nail, and blood	ICP-MS	Zn, Cu, and Se (not specified)	Samples were dried at 90 °C and then weighed and the digestion involved 0.5 mL of 65% trace metal grade nitric acid, heated to 80 °C in a dry bath incubator, using 0.05–0.10 g of the samples. After digestion, the samples were diluted to a final volume of 1.0 mL with a 1% HNO_3 solution, and a gallium internal standard solution was added before analysis	[167]
Finger and toenails	ICP-Q-MS	U, Pu, and Am	Microwave digestion system was utilized to process hair and nail samples, with each sample being treated with 3.1 mL of concentrated HNO_3 at 180 °C for 15 min. After digestion, the solutions were diluted to a 6 M HNO_3 concentration using 8.0 mL of ultra-high purity water, and enhanced with trace amounts of ^{242}Pu and ^{243}Am for isotopic analysis	[168]
Rat tissues	ICP-MS	Pt (3 ng/mL)	The Pt standard solution was diluted with a 2% HNO_3 solution prior to use. For plasma analysis, a 0.1 mL aliquot was digested by adding 3 mL of concentrated nitric acid and heated at 180 °C on a hot plate for one hour to achieve complete dissolution. After cooling, 0.6 mL of hydrogen peroxide was introduced and the mixture was reheated to precipitate solids. The volume was reduced through evaporation to 0.5 mL, after which it was diluted with a 2% nitric acid solution to reach a final volume of 10 mL for platinum measurement. Tissue samples followed a similar procedure but required 2 mL of concentrated nitric acid for every 0.1 g of tissue during the digestion phase	[169]

Table 4 (continued)

Biological Samples	ICP-MS Technique	Elements & Limit of detection (LOD)	Preparation & Matrix/ Background	Ref
Fish tissues (muscle, skin, and liver)	ICP-MS	Hg (0.006), Ni (0.35), Cu (0.20), Pb (0.07), Cr (0.33), Cd (0.004), Mn (0.35), As (0.035), and Se (0.035)—all measured as μg kg^{-1}	Concentrated nitric acid at 65% concentration was utilized to digest fish tissue samples. Element-specific working solutions were prepared from 1000 mg/L stock along with a 10 mg/L iridium solution	[170]
Tumor tissues	LA-ICP-MS	Zn (imaging)	Tumor samples were transferred on an aluminum block cooled by liquid nitrogen and placed in a cryoablation chamber at −15 °C, purged with helium to eliminate oxygen and water. Zinc quantification utilized a matrix-adapted calibration method with a 12.5% polyacrylamide gel spiked with a zinc standard solution before polymerization. Key measurement parameters included a laser spot size of 200 μm, a 20 μm ablation line overlap, a 50 μm/s ablation speed, and a 1 s ICP-MS sampling time, achieving a final image resolution of 180 × 50 μm^2	[171]
Mouse tissues	LA-ICP-(TOF)MS	P, Fe, Cu (imaging)	Ultrapure water and nitric acid were utilized for all standard solution dilutions, with a multi-element stock. Gelatin-based micro-droplet standards were prepared in three variations: multi-element in nitric acid, single-element in hydrofluoric and nitric acid, and single-element in hydrochloric acid, all serially diluted appropriately. These standards were spotted onto glass slides using a cellenONE X1 micro-spotter, producing droplets with volumes of approximately 370 pL and diameters of 150–200 μm	[172]
Thyroid tissues	ICP-MS	Ni, As, Pb, Cd, and U (not specified)	High-grade nitric acid (65%) and hydrogen peroxide (30%) were used for sample digestion, with the nitric acid further purified using a Berghof-acid device (BSB-939-IR). Approximately 0.70 g of each clinical sample was measured precisely before being decomposed in a 4:1 (v/v) mixture of nitric acid and hydrogen peroxide at 180 ºC using a microwave system. After cooling, the decomposed samples were transferred and diluted to a final volume of 25 mL with ultrapure water (18.2 MΩ resistance from a Milli-Q plus system, Merck). The diluted internal standard solution was prepared from stock solutions (100 mg/L 7Li, Sc; 20 mg/L Bi, Ga, In, Tb, Y). Calibration was achieved using solutions ranging from 0.1 to 250 μg/L, achieving an R-value greater than 0.9993	[173]

Table 4 (continued)

Biological Samples	ICP-MS Technique	Elements & Limit of detection (LOD)	Preparation & Matrix/ Background	Ref
Thyroid tissues	ICP-MS	As, Cd, Pb, Mn, Cu, Zn, and Se (not specified)	Approximately 0.5 g of thyroid tissue was weighed and placed in a microwave cuvette. The sample underwent digestion at 180 °C using 4 mL of concentrated nitric acid and 1 mL of hydrogen peroxide. The digestion process involved a 10-min warm-up to 180 °C, followed by an additional 15 min of heating. After cooling, the decomposed samples were transferred quantitatively into 25-mL volumetric flasks and diluted with ultrapure water. Analytical standards included a multi-element stock solution (10 mg/L) Four internal standards—45Sc at 50 µg/L, and Y, Tb, and Bi at 10 µg/L—were employed to adjust for matrix effects and instrument drift	[174]
Mammalian organ issues and blood	ICP-MS	Ag, Al, As, Ba, Be, Ca, Cd, Co, Cr, Cs, Cu, Fe, Ga, K, Li, Mg, Mn, Na, Ni, Pb, Rb, Se, Sr, Tl, U, V, and Zn (not specified)	Tissue and serum samples underwent acidic treatment using a microwave digestion system, with 30–80 mg of tissue dissolved in 10 ml of 65% nitric acid and 100–200 ml of serum prepared for digestion. The microwave digestion operated at a gradual increase to 150 °C over 15 min, maintained for 30 min. This method was optimized after observing equipment shutdowns at temperatures above 200 °C, establishing that a medium temperature and 500W power setting sufficed for sample digestion. Post-digestion, samples were stored at −20 °C until analyzed. For standard preparation, a multi-element solution containing various elements at 10 ppm in a 5% nitric acid matrix served as the external calibration standard, with a 2% nitric acid solution used as the blank	[175]
Whole body blood	ICP-MS	Al (2.0), Bi (0.02), Ce (0.02), Cr (0.7), Ge (0.1), La (0.03), Li (0.2), Nd (0.01), Pr (0.01), Te (0.2), Ti (5.0) and Y (0.02)—all measured in µg/L	Dilution of blood samples with a 0.7% nitric acid and 0.1% Triton X-100 solution, with Rhodium and Terbium used as internal standards to enhance measurement accuracy. The diluted samples were centrifuged, and the supernatant was then analyzed for a spectrum of elements. For effective calibration and reduction of matrix effects, the samples were prepared in a solution that mimicked the blood matrix, consisting of nitric acid, Triton X-100, potassium, and isopropyl alcohol	[176]
Horse whole blood	ICP-Q-MS	Ag (0.001), Al (0.081), As, 90.001), B (0.003), Ba (0.002), Be (0.005), Bi (0.001), Cd (0.001), Co (0.001), Cr (0.001), Cu (0.015), Fe (0.014), Hg (0.001), K (0.221), Li (0.003), Mg (0.037), Mn (0.001), Mo (0.002), Na (1.323), Ni (0.008), Pb (0.001), Sb (0.001), Se (0.062), Sr (0.004), Ti (0.001), Tl (0.001), V (0.001), and Zn (0.057)—all measured in µg/kg	Samples were collected using vacuum tubes containing K3-EDTA and stored at a refrigeration temperature of 4 °C. For analysis, 0.25 g of whole blood was mixed with 1 mL of 0.5 mg L^{-1} internal Re standard, digested in 8 mL of 70% HNO3 and 3 mL H2O using a microwave mineralizer system. Similarly, about 0.50 g of hay and concentrates were digested with 7 mL of 69% HNO_3 and 2 mL of 30% H_2O_2. After digestion, samples were adjusted to 25 mL with ultrapure water, and water samples were diluted with 2% nitric acid	[177]

Table 4 (continued)

Biological Samples	ICP-MS Technique	Elements & Limit of detection (LOD)	Preparation & Matrix/ Background	Ref
Human blood	ICP-MS	As Cd, Co, Cr, Mn, and Pb —0.2 µg/L across the measured elements	The digestion of the samples involved using perchloric and nitric acid in a 1:3 ratio, specifically adding 3 mL of perchloric acid and 9 mL of Suprapur® concentrated nitric to 1 g of each sample in a quartz tube, followed by vortexing for 30 s. The samples were then treated with a mixture of 0.5% HCl and 1.5% HNO_3 in purified water, diluted, and centrifuged to separate the supernatants for ICP-MS analysis. To ensure accuracy and reliability, samples were processed in triplicate. Quality control was maintained using internal standards (2.50 µg/L indium, 0.25 µg/L terbium, 50 µg/L yttrium, all in 0.5% HNO_3) and external certified reference materials (ClinChek®) specific to the metals being analyzed	[178]
Dried blood spots	ICP-MS	Hg (0.10 µg/L for a volume of 50 µL)	Blood samples were gently mixed for homogenization and diluted 1:50 in an aqueous solution containing 10 ppb rhodium as an internal standard, 0.05% Triton X-100 (v/v), 0.05% EDTA (v/v), 10% propanol (v/v), 10 µg/L H(AuCl4), and 1% tetramethylammonium hydroxide (TMAH) (v/v). Internal quality controls were systematically applied, using Seronorm® Trace Elements Whole Blood levels 1 and 2, at the beginning, end, and after every ten samples analyzed	[179]
Whole blood	ICP-MS	Ag (0.04), As (0.06), Bi (0.04), Cd (0.2), Co (0.06), Cr (1.8), Cu (0.6), Hg (0.2), I (0.4), Mn (0.2), Mo (0.2), Ni (0.8), Pb (0.2), Se (0.2), Tl (0.02), U (0.04), V (0.2), Zn (4)—all measured in mg/kg	Blood samples were then combined with an alkaline solution using a Vortex Mixer from the same manufacturer. To avoid contamination, all laboratory equipment, including 10 mL plastic tubes and caps was acid-washed by immersing them in 10% nitric acid for a minimum of 24 h. In preparation, a 0.25 mL aliquot of each homogenized sample was placed into an acid-washed 10 mL tube, mixed with 0.5 mL of alkaline solution, and diluted to a final volume of 5 mL, achieving a 20-fold dilution. This mixture was then thoroughly vortexed for optimal decomposition. The alkaline solution itself was prepared in a 500 mL plastic bottle, combining 5 g of EDTA, 50 mL of ammonia solution, 50 mL of isopropanol, and 5 mL of Triton X-100	[180]
Whole blood	ICP-MS	Na (1341,30), Mg (759,70), K (473,00), Ca (127, 80), Mn (0,70), Fe (36, 80), Cu (2,20), Zn (7,10) and Se (12,00)—all measured in µg/L	Initially, 100 µl of either serum or whole blood from the ClinCheck control was transferred into a 15 ml polypropylene tube with a screw cap. To this, 200 µl of roughly 65% nitric acid (HNO_3) and 100 µl of hydrogen peroxide (H_2O_2) were added, and the mixture was briefly vortexed. The tubes were then placed in a heating system set at 60°C for a dissolution period of 90 min. Following incubation, the samples were cooled by introducing 2100 µl of ultrapure water (RT)	[22]

units are not suitable for most on-site measurements. Portable XRF analyzers, on the other hand, provide considerable flexibility by allowing for in-field measurements. Although they do not match the sensitivity of benchtop models, they can provide immediate results which make them especially useful for preliminary surveys and field studies where mobility is a key requirement and low concentrations of elements are not a concern [86, 91, 94, 95, 97, 102, 145, 146, 181].

- **Limits of Detection:** ICP-MS is renowned for its incredibly low detection limits (ppt) of almost any element within a sample [46]. XRF generally has detection limits in the ppm to ppb range but is still effective for broader screening purposes where extreme sensitivity is less critical [155]. TRXRF can reach ppt-level detection but only for liquid samples [182].
- **Required Expertise:** ICP-MS requires specialized expertise for both instrument operation and complex sample preparation. XRF's simpler operation and lower training requirements make it more accessible for routine use by a broader range of personnel.
- **Cost:** The operational costs and initial investment associated with ICP-MS are significant, encompassing a high initial investment (typically $200 k-$500 k) in equipment but also ongoing expenses for consumables, maintenance, and operation within a controlled lab environment. XRF is generally less expensive (typically $30 k-150 k), requiring fewer consumables and less specialized training, making it a more cost-effective option for routine analyses.

Conclusion and Future Prospects

This review explored the strengths and limitations of ICP-MS and XRF technologies for quantifying metals in biological samples. ICP-MS is acclaimed for its ppt sensitivity, making it indispensable for toxicological studies and environmental monitoring; however, its complexity, cost, and extensive sample preparation can limit its applicability where rapid turnaround or sample preservation is necessary. XRF stands out for its non-destructive nature and minimal sample preparation, allowing rapid, on-site analysis within seconds to minutes. This makes XRF advantageous for field studies, preliminary surveys requiring immediate results, and studies where extreme trace detection is not critical.

Factors like sensitivity, precision, speed, cost-efficiency, and the physical nature of the samples should guide the choice between these technologies. For instance, portable XRF devices offer mobility and ease of use for in-field applications but are less sensitive than ICP-MS. Conversely, ICP-MS systems and their high cost, power needs, time-consuming sample preparation, and slower speed, are better suited for detailed quantitative analysis in controlled laboratory environments.

The use of these analytical techniques will improve health risk assessments, environmental monitoring, and the diagnosis and treatment of metal-related diseases. While both ICP-MS and XRF have distinct advantages and limitations, their continuous development is crucial for meeting the growing demands of scientific research and public health, enhancing our understanding of metal dynamics in biological and environmental systems.

Acknowledgements The authors extend additional gratitude to laboratory undergraduate mentees, Jessie M. Lanzer and Stefano A. Parducci, for their invaluable support in aiding parts of this review

Author Contribution K. E. Adesina: Conceptualization, Methodology, Formal analysis, Visualization, Writing-original draft, Writing-review & editing. C. J. Burgos: Visualization, Writing-review & editing. T. R. Grier: Visualization, Writing-review & editing. A. S. M. Sayam: Visualization, Writing-review & editing. A. J. Specht: Conceptualization, Methodology, Validation, Funding, Visualization, Writing-original draft, Writing-review & editing.

Data Availability No datasets were generated or analysed during the current study.

Declarations

Human and Animal Rights and Informed Consent This article does not contain any studies with human or animal subjects performed by any of the authors.

Conflict of Interest The authors declare no competing interests.

References

1. Xiang P, Han Y-H, Li H-B, Gao P. Editorial: advanced analytical techniques for heavy metals speciation in soil, crop, and human samples. Front Chem. 2023;11:1151371.
2. Custódio PJ, Carvalho ML, Nunes F, Pedroso S, Campos A. Direct analysis of human blood (mothers and newborns) by energy dispersive X-ray fluorescence. J Trace Elem Med Biol. 2005;19:151–8.
3. Ekinci R, Ekinci N. An alternative method for the determination of element concentrations in schizophrenic, lung cancer and leukaemia patient bloods. J Quant Spectrosc Radiat Transf. 2004;86:379–85.
4. Yip CWY, Ho JPY, Nikezic D, Yu KN. A fast method to measure the thickness of removed layer from etching of SSNTD based on EDXRF. Radiat Meas. 2003;36:161–4.
5. Wróbel A, Goncerz G, Kunz J, Podolec P, Rokita E. Effect of gallium on in vitro aortic valve cusp mineralization – EDXRF studies. Nucl Instrum Methods Phys Res B. 2004;213:556–9.
6. Miskolczi N, Bartha L, Antal F, Dudas C. Determination of sulphur in liquids obtained by thermal cracking of waste polymers and commercial fuels with different analytical methods. Talanta. 2005;66:1264–71.
7. Obiajunwa EI, Pelemo DA, Owolabi SA, Fasasi MK, Johnson-Fatokun FO. Characterisation of heavy metal pollutants of soils

and sediments around a crude-oil production terminal using EDXRF. Nucl Instrum Methods Phys Res B. 2002;194:61–4.
8. Anjos MJ, Lopes RT, Jesus EFO, Assis JT, Cesareo R, Barroso RC, Barradas CAA. Elemental concentration analysis in soil contaminated with recyclable urban garbage by tube-excited energy-dispersive X-ray fluorescence. Radiat Phys Chem. 2002;65:495–500.
9. Egunjobi KA, Adesina KE, Chime IP. Radiological assessment of soil samples from selected dumpsites in Mowe. CCU J Sci. 2020;1:72–80.
10. Oyedele OO, Olaniyan DS, Gabriel JA, Abejide FH, Adesina KE. Assessing the environmental risk of heavy metals in surrounding areas of Lafarge Cement Industry in Shagamu, Ogun State, Nigeria. Chem Environ Sci Arch. 2023;03:40–7.
11. Bolann BJ, Rahil-Khazen R, Henriksen H, Isrenn R, Ulvik RJ. Evaluation of methods for trace-element determination with emphasis on their usability in the clinical routine laboratory. Scand J Clin Lab Invest. 2007;67:353–66.
12. Jiang L, Huang J, Wang Y, Tang H. Eliminating the dication-induced intersample chemical-shift variations for NMR-based biofluid metabonomic analysis. Analyst. 2012;137:4209.
13. Ammerman J, Huang C, Sailstad J, et al. Technical aspects of inductively coupled plasma bioanalysis techniques. Bioanalysis. 2013;5:1831–41.
14. Wilschefski S, Baxter M. Inductively coupled plasma mass spectrometry: introduction to analytical aspects. Clin Biochem Rev. 2019;40:115–33.
15. Konz T, Monnard C, Restrepo MR, et al. Multielemental analysis of low-volume samples reveals cancer-specific profile in serum and sorted immune cells. Anal Chem. 2020;92:8750–8.
16. Rodushkin I, Axelsson MD. Application of double focusing sector field ICP-MS for multielemental characterization of human hair and nails. Part II. A study of the inhabitants of northern Sweden☆. Sci Total Environ. 2000;262:21–36.
17. Morton J, Tan E, Suvarna SK. Multi-elemental analysis of human lung samples using inductively coupled plasma mass spectrometry. J Trace Elem Med Biol. 2017;43:63–71.
18. Joda BA, Ward NI. Use of human teardrop fluid for the determination of trace elements in healthy individuals and diabetic patients. J Trace Elem Med Biol. 2021;65:126733.
19. Morton J, Tan E, Leese E, Cocker J. Determination of 61 elements in urine samples collected from a non-occupationally exposed UK adult population. Toxicol Lett. 2014;231:179–93.
20. Tanvir EM, Whitfield KM, Ng JC, Shaw PN. Development and validation of an ICP-MS method and its application to determine multiple trace elements in small volumes of whole blood and plasma. J Anal Toxicol. 2021;44:1036–46.
21. Meyer S, Markova M, Pohl G, Marschall TA, Pivovarova O, Pfeiffer AFH, Schwerdtle T. Development, validation and application of an ICP-MS/MS method to quantify minerals and (ultra-)trace elements in human serum. J Trace Elem Med Biol. 2018;49:157–63.
22. Laur N, Kinscherf R, Pomytkin K, Kaiser L, Knes O, Deigner H-P. ICP-MS trace element analysis in serum and whole blood. PLoS ONE. 2020;15:e0233357.
23. Liu Y, Xiao G, Jones RL. Rapid determination of thorium in urine by quadrupole inductively coupled plasma mass spectrometry (Q-ICP-MS). J Radioanal Nucl Chem. 2022;331:3957–64.
24. Ferella F, Nisi S, Balata M, Grabmayr P, Laubenstein M, Schwingenheuer B, Schönert S. Enriched high purity germanium detectors for the LEGEND-200 experiment: purification and characterization by quadrupole and high resolution inductively coupled plasma mass spectrometry (ICP-MS). Appl Radiat Isot. 2023;200:110904.
25. Catarino S, Thanasi V, Morin G, Anjos O, Fernandes TA, Caldeira I, Fargeton L, Boissier B, Canas S. Shedding light on metals release from Chestnut Wood to Wine spirit using ICP-MS. Foods. 2022;11:3617.
26. Wilschefski S, Baxter M, Pool G. A simple equation to correct for gadolinium interference on plasma selenium measurement using inductively coupled plasma mass spectrometry. Ann Clin Biochem. 2020;57:234–41.
27. Simić A, Hansen AF, Syversen T, Lierhagen S, Ciesielski TM, Romundstad PR, Midthjell K, Åsvold BO, Flaten TP. Trace elements in whole blood in the general population in Trøndelag County, Norway: the HUNT3 survey. Sci Total Environ. 2022;806:150875.
28. Montrose L, Goodrich JM, Morishita M, Kochmanski J, Klaver Z, Cavalcante R, Lumeng JC, Peterson KE, Dolinoy DC. Neonatal lead (Pb) exposure and DNA methylation profiles in dried bloodspots. Int J Environ Res Public Health. 2020;17:6775.
29. Swiatkowska I, Martin NG, Henckel J, Apthorp H, Hamshere J, Hart AJ. Blood and plasma titanium levels associated with well-functioning hip implants. J Trace Elem Med Biol. 2020;57:9–17.
30. Koski L, Berntsson E, Vikström M, Wärmländer SKTS, Roos PM. Metal ratios as possible biomarkers for amyotrophic lateral sclerosis. J Trace Elem Med Biol. 2023;78:127163.
31. Sproson AD, Aze T, Behrens B, Yokoyama Y. Initial measurement of beryllium-9 using high-resolution inductively coupled plasma mass spectrometry allows for more precise applications of the beryllium isotope system within the Earth Sciences. Rapid Commun Mass Spectrom. 2021. https://doi.org/10.1002/rcm.9059.
32. Irigoyen-Arredondo MS, Moreno-Sánchez XG, Escobar-Sánchez O, Soto-Jiménez MF, Marín-Enríquez E, Abitia-Cárdenas LA. Essential (Cu, Zn) and nonessential (Pb, Cd) metals in the muscle of leopard groupers (Mycteroperca rosacea) from a mining port in the Gulf of California, Mexico: human health risk assessment. Environ Sci Pollut Res. 2022;29:35001–11.
33. Echeverría R, Vrhovnik P, Salcedo-Bellido I, Iribarne-Durán LM, Fiket Ž, Dolenec M, Martin-Olmedo P, Olea N, Arrebola JP. Levels and determinants of adipose tissue cadmium concentrations in an adult cohort from Southern Spain. Sci Total Environ. 2019;670:1028–36.
34. Rani N, Sastry BS, Dey K. Assessment of metal contamination and the associated human health risk from dustfall deposition: a study in a mid-sized town in India. Environ Sci Pollut Res. 2019;26:23173–91.
35. Bačić N, Mikac N, Lučić M, Sondi I. Occurrence and distribution of technology-critical elements in recent freshwater and marine pristine lake sediments in Croatia: a case study. Arch Environ Contam Toxicol. 2021;81:574–88.
36. Arı B, Bakırdere S. A primary reference method for the characterization of Cd, Cr, Cu, Ni, Pb and Zn in a candidate certified reference seawater material: TEA/Mg(OH)2 assisted ID3MS by triple quadrupole ICP-MS/MS. Anal Chim Acta. 2020;1140:178–89.
37. Kneer ML, Lazarcik J, Ginder-Vogel M. Investigation of ICP-MS/MS for total sulfur quantification in freshwater dissolved organic matter. J Environ Qual. 2021;50:1476–85.
38. Yang HS, LaFrance DR, Hao Y. Elemental testing using inductively coupled plasma mass spectrometry in clinical laboratories. Am J Clin Pathol. 2021;156:167–75.
39. Arı B, Can SZ, Bakırdere S. Traceable and accurate quantification of iron in seawater using isotope dilution calibration strategies by triple quadrupole ICP-MS/MS: Characterization measurements of iron in a candidate seawater CRM. Talanta. 2020;209:120503.

40. Vezzulli F, Fontanella MC, Lambri M, Beone GM. Specialty and high-quality coffee: discrimination through elemental characterization via ICP - OES, ICP - MS, and ICP - MS/MS of origin, species, and variety. J Sci Food Agric. 2023;103:4303–16.
41. Bohn MK, Nichols M, Yang L, Bhayana V, Macri J, Adeli K. Pediatric reference value profiling of essential trace and toxic elements in healthy children and adolescents using high-resolution and triple quadrupole inductively coupled plasma mass spectrometry. J Appl Lab Med. 2023;8:674–88.
42. Melczer M, Jiménez Lamana J, Justo-Vega A, Hanser O, Ndaw S, Lobinski R. Multielement analysis of single red blood cells by single cell - inductively coupled plasma tandem mass spectrometry. Talanta. 2024;267:125226.
43. Belkouteb N, Schroeder H, Arndt J, Wiederhold JG, Ternes TA, Duester L. Quantification of 68 elements in river water monitoring samples in single-run measurements. Chemosphere. 2023;320:138053.
44. Schmidt L, Peterson K, Nunes TS, Knap M, Petrick L, Landero-Figueroa JA. A miniaturized sample preparation method for routine elemental determination in whole blood using volumetric absorptive micro-sampling by ICP-QQQ. Anal Bioanal Chem. 2023. https://doi.org/10.1007/s00216-023-04881-7.
45. Wu Y, Chao Y, Miao Y, Li Y, Xu T, Li S, Peng J. Time-resolved ICP-MS analysis of mineral element contents and distribution patterns in spermatogenic cells of different types. Anal Chim Acta. 2023;1255:341054.
46. Tian X, Jiang H, Wang M, et al. Exploring the performance of quadrupole, time-of-flight, and multi-collector ICP-MS for dual-isotope detection on single nanoparticles and cells. Anal Chim Acta. 2023;1240:340756.
47. Chun K-H, Lum JT-S, Leung KS-Y. Dual-elemental analysis of single particles using quadrupole-based inductively coupled plasma-mass spectrometry. Anal Chim Acta. 2022;1192:339389.
48. Zheng Z, Wei Q, Wan X, Zhong X, Liu L, Zeng J, Mao L, Han X, Tou F, Rao J. Correlation analysis between trace elements and colorectal cancer metabolism by integrated serum proteome and metabolome. Front Immunol. 2022. https://doi.org/10.3389/fimmu.2022.921317.
49. Aynard A, Courrèges C, Jiménez-Lamana J, Raad A, Miqueu C, Grassl B, Reynaud S. Trace metal sorption on nanoplastics: an innovative analytical approach combining surface analysis and mass spectrometry techniques. Environ Pollut. 2023;323:121229.
50. Theiner S, Schweikert A, Van Malderen SJM, Schoeberl A, Neumayer S, Jilma P, Peyrl A, Koellensperger G. Laser Ablation-Inductively Coupled Plasma Time-of-Flight Mass Spectrometry Imaging of Trace Elements at the Single-Cell Level for Clinical Practice. Anal Chem. 2019;91:8207–12.
51. Brown RJC, Jarvis KE, Disch BA, Goddard SL, Adriaenssens E, Claeys N. Comparison of ED-XRF and LA-ICP-MS with the European reference method of acid digestion-ICP-MS for the measurement of metals in ambient particulate matter. Accred Qual Assur. 2010;15:493–502.
52. Ishii C, Nakayama SMM, Kataba A, et al. Characterization and imaging of lead distribution in bones of lead-exposed birds by ICP-MS and LA-ICP-MS. Chemosphere. 2018;212:994–1001.
53. Chen J, Wang R, Ma M, Gao L, Zhao B, Xu M. Laser ablation–inductively coupled plasma–mass spectrometry (LA-ICP-MS)–based strategies applied for the analysis of metal-binding protein in biological samples: an update on recent advances. Anal Bioanal Chem. 2022;414:7023–33.
54. Li F, Cui H, Zhang D, Li H, Guo W, Jin L, Hu S. Direct multi-elemental analysis of cerebrospinal fluid samples by LA-ICP-MS employing an aerosol local extraction cryogenic ablation cell. Anal Bioanal Chem. 2023;415:6051–61.
55. Martinez M, Baudelet M. Calibration strategies for elemental analysis of biological samples by LA-ICP-MS and LIBS – A review. Anal Bioanal Chem. 2020;412:27–36.
56. Fernandes ACBCJ, Yang P, Armstrong D, França R. Metal distributions in human hair strand cross-section: advanced analysis using LA-ICP-MS in dentistry. Talanta. 2023;265:124909.
57. Stepka P, Kratochvilova M, Kuchynka M, Raudenska M, Polanska HH, Vicar T, Vaculovic T, Vaculovicova M, Masarik M. Determination of renal distribution of Zinc, Copper, Iron, and Platinum in Mouse Kidney using LA-ICP-MS. Biomed Res Int. 2021;2021:1–8.
58. Torimoto R, Ishii C, Sato H, et al. Analysis of lead distribution in avian organs by LA-ICP-MS: Study of experimentally lead-exposed ducks and kites. Environ Pollut. 2021;283:117086.
59. Folarin OR, Olopade FE, Olopade JO. Essential metals in the Brain and the application of laser ablation-inductively coupled plasma-mass spectrometry for their detection. Niger J Physiol Sci. 2021;36:123–47.
60. LaBine GO, Molloy PP, Christensen JR. Determination of elemental composition in soft biological tissue using laser ablation inductively coupled plasma mass spectrometry: method validation. Appl Spectrosc. 2021;75:1262–77.
61. Von der Au M, Karbach H, Bell AM, Bauer OB, Karst U, Meermann B. Determination of metal uptake in single organisms, Corophium volutator, via complementary electrothermal vaporization/inductively coupled plasma mass spectrometry and laser ablation/inductively coupled plasma mass spectrometry. Rapid Commun Mass Spectrom. 2021. https://doi.org/10.1002/rcm.8953.
62. Van Grieken RE, Markowicz A. Handbook of X-Ray Spectrometry, 2e. New York: Marcel Dekker Inc.; 1993.
63. Goulding FS, Jaklevic JM. Photon-excited energy-dispersive X-Ray fluorescence analysis for trace elements. Annu Rev Nucl Sci. 1973;23:45–74.
64. Specht AJ, Obrycki JF, Mazumdar M, Weisskopf MG. Feasibility of lead exposure assessment in blood spots using energy-dispersive X-ray fluorescence. Environ Sci Technol. 2021;55:5050–5.
65. Kinoshita H, Tanaka N, Jamal M, Kumihashi M, Okuzono R, Tsutsui K, Ameno K. Application of energy dispersive X-ray fluorescence spectrometry (EDX) in a case of methomyl ingestion. Forensic Sci Int. 2013;227:103–5.
66. Stump IG, Carruthers J, D'Auria JM, Applegarth DA, Davidson AGF. Quantitative analysis of trace elements in human blood and plasma by energy dispersive X-ray fluorescence. Clin Biochem. 1977;10:127–32.
67. Van Loggerenberg DE, Laver PN, Myburgh JG, Botha CJ. Diagnostic value of energy dispersive hand-held X-ray Fluorescence spectrometry in determining trace element concentrations in ovine liver. Biol Trace Elem Res. 2019;190:358–61.
68. Marguí E, Queralt I, Hidalgo M. Determination of cadmium at ultratrace levels in environmental water samples by means of total reflection X-ray spectrometry after dispersive liquid–liquid microextraction. J Anal At Spectrom. 2013;28:266–73.
69. Marguí E, Sagué M, Queralt I, Hidalgo M. Liquid phase microextraction strategies combined with total reflection X-ray spectrometry for the determination of low amounts of inorganic antimony species in waters. Anal Chim Acta. 2013;786:8–15.
70. Cordero MO, Barreda MFG. Sampling and sample preparation for chemical analysis of plants by wavelength dispersive X-Ray fluorescence. In: X-Ray fluorescence in biological sciences. Wiley; 2022. pp. 443–466. https://doi.org/10.1002/9781119645719.ch29.
71. San Diego: Eurofins EAG Laboratories. Our Techniques [internet]. 2015. https://www.eag.com/techniques. Accessed 26 Mar 2024.

72. Haschke M, Boehm S. Micro-XRF in scanning electron microscopes. 2017;1–60. https://doi.org/10.1016/bs.aiep.2017.01.001.
73. Haschke M. Micro-X-ray fluorescence-Instrumentation and application. Berlin: Springer; 2014.
74. Mishra NL, Dhara S. Total reflection X-Ray fluorescence and it's suitability for biological samples. In: X-Ray fluorescence in biological sciences. Wiley; 2022. pp. 61–72. https://doi.org/10.1002/9781119645719.ch4.
75. Rodríguez-Saldaña V, Fobil J, Basu N. Lead (Pb) exposure assessment in dried blood spots using Total Reflection X-Ray Fluorescence (TXRF). Environ Res. 2021;198:110444.
76. Tiwari MK. Elemental analysis using synchrotron radiation X-Ray Fluorescence. In: X-Ray Fluorescence in Biological Sciences. Wiley, 2022. pp. 115–149.
77. Hu H, Zhao J, Wang L, Shang L, Cui L, Gao Y, Li B, Li Y-F. Synchrotron-based techniques for studying the environmental health effects of heavy metals: Current status and future perspectives. TrAC Trends Anal Chem. 2020;122:115721.
78. Groskopf C, Bennett SR, Gherase MR, Fleming DEB. Detection of lead in bone phantoms and arsenic in soft tissue phantoms using synchrotron radiation and a portable x-ray fluorescence system. Physiol Meas. 2017;38:374–86.
79. Janssens K, Adams FCV, Rindby A. Micro-X-ray fluorescence analysis. Wiley; 2000. p. 434.
80. Trunova VA. Synchronous Radiation X-Ray Fluorescence Analysis of Microelements in Biopsy Tissues. In: X-Ray Fluorescence in Biological Sciences. Wiley, 2022. pp. 183–201.
81. Julshamn K, Utne F, Braekkan OR. Interactions of Cadmium with Copper, Zinc and iron in different organs and tissues of the Rat. Acta Pharmacol Toxicol (Copenh). 2009;41:515–24.
82. Bachvarova D, Stancheva M, Ignatova-Ivanova T, Ibryamova S, Chipev N, Alexandrova A. Trace metal accumulation in tissues of wedge clams from sandy habitats of the Bulgarian Black Sea coast. BioRisk. 2022;2022:73–81.
83. Bali V, Khajuria Y, Maniyar V, Rai PK, Kumar U, Ghany C, Gondal MA, Singh VK. Quantitative analysis of human hairs and nails. Biophys Rev. 2023;15:401–17.
84. Frederickson CJ, Fleming DEB, Asael D, et al (2023) Single hair analysis by X-ray fluorescence spectrometry detects small changes in dietary zinc intake: a nested randomized controlled trial. Front Nutr. https://doi.org/10.3389/fnut.2023.1139017.
85. Cloete KJ, Šmit Ž, Gianoncelli A. Multidimensional profiling of human body hairs using qualitative and semi-quantitative approaches with SR-XRF, ATR-FTIR, DSC, and SEM-EDX. Int J Mol Sci. 2023;24:4166.
86. Bhatia M, Specht AJ, Ramya V, Sulaiman D, Konda M, Balcom P, Sunderland EM, Qureshi A. Portable X-ray fluorescence as a rapid determination tool to detect parts per million levels of Ni, Zn, As, Se, and Pb in human toenails: a south india case study. Environ Sci Technol. 2021;55(19):13113–21.
87. Zhang X, Specht AJ, Weisskopf MG, Weuve J, Nie LH. Quantification of manganese and mercury in toenail *in vivo* using portable X-ray fluorescence (XRF). Biomarkers. 2018;23:154–60.
88. Specht AJ, Zhang X, Young A, Nguyen VT, Christiani DC, Ceballos DM, Allen JG, Weuve J, Nie LH, Weisskopf MG. Validation of in vivo toenail measurements of manganese and mercury using a portable X-ray fluorescence device. J Expo Sci Environ Epidemiol. 2022;32:427–33.
89. Gutiérrez-González E, García-Esquinas E, de Larrea-Baz NF, Salcedo-Bellido I, Navas-Acien A, Lope V, Gómez-Ariza JL, Pastor R, Pollán M, Pérez-Gómez B. Toenails as biomarker of exposure to essential trace metals: a review. Environ Res. 2019;179:108787.
90. Specht AJ, Adesina KE, Read DE, Weisskopf MG. Benchtop x-ray fluorescence to quantify elemental content in nails non-destructively. Sci Total Environ. 2024;918:170601.
91. Specht AJ, Dickerson AS, Weisskopf MG. Comparison of bone lead measured via portable x-ray fluorescence across and within bones. Environ Res. 2019;172:273–8.
92. Specht AJ, Parish CN, Wallens EK, Watson RT, Nie LH, Weisskopf MG. Feasibility of a portable X-ray fluorescence device for bone lead measurements of condor bones. Sci Total Environ. 2018;615:398–403.
93. Specht AJ, Weisskopf M, Nie LH. Portable XRF technology to quantify Pb in bone *In Vivo*. J Biomark. 2014;2014:1–9.
94. Hampton JO, Specht AJ, Pay JM, Pokras MA, Bengsen AJ. Portable X-ray fluorescence for bone lead measurements of Australian eagles. Sci Total Environ. 2021;789:147998.
95. Specht AJ, Mostafaei F, Lin Y, Xu J, Nie LH. Measurements of Strontium levels in human bone In Vivo using portable X-ray Fluorescence (XRF). Appl Spectrosc. 2017;71:1962–8.
96. Kim R, Aro A, Rotnitzky A, Amarasiriwardena C, Hu H. K X-ray fluorescence measurements of bone lead concentration: the analysis of low-level data. Phys Med Biol. 1995;40:1475–85.
97. Zhang X, Specht AJ, Wells E, Weisskopf MG, Weuve J, Nie LH. Evaluation of a portable XRF device for in vivo quantification of lead in bone among a US population. Sci Total Environ. 2021;753:142351.
98. Moise H, Chettle DR, Pejović-Milić A. Monitoring bone strontium intake in osteoporotic females self-supplementing with strontium citrate with a novel in-vivo X-ray fluorescence based diagnostic tool. Bone. 2014;61:48–54.
99. Specht AJ, Lin Y, Weisskopf M, Yan C, Hu H, Xu J, Nie LH. XRF-measured bone lead (Pb) as a biomarker for Pb exposure and toxicity among children diagnosed with Pb poisoning. Biomarkers. 2016;21:347–52.
100. Kalnicky DJ, Singhvi R. Field portable XRF analysis of environmental samples. J Hazard Mater. 2001;83:93–122.
101. McIntosh KG, Guimarães D, Cusack MJ, Vershinin A, Chen ZW, Yang K, Parsons PJ. Evaluation of portable XRF instrumentation for assessing potential environmental exposure to toxic elements. Int J Environ Anal Chem. 2016;96:15–37.
102. Nzabanita D, Hampton JO, Toop SD, Bengsen AJ, Specht AJ, Flesch JS, Hufschmid J, Nugegoda D. Expanding the use of portable XRF to monitor lead exposure in an Australian duck species two decades after a ban on lead shot. Sci Total Environ. 2023. https://doi.org/10.1016/j.scitotenv.2023.161803.
103. Totten MS, Davenport TS, Edwards LF, Howell JM. Trace minerals and anxiety: a review of Zinc, Copper, Iron, and Selenium. Dietetics. 2023;2:83–103.
104. World Health Organization. Human biomonitoring: Facts and figures. WHO Regional Office for Europe, Copenhagen. 2015. www.euro.who.int. Accessed 26 Mar 2024.
105. Ganzleben C, Antignac J-P, Barouki R, et al. Human biomonitoring as a tool to support chemicals regulation in the European Union. Int J Hyg Environ Health. 2017;220:94–7.
106. Zidek A, Macey K, MacKinnon L, Patel M, Poddalgoda D, Zhang Y. A review of human biomonitoring data used in regulatory risk assessment under Canada's Chemicals Management Program. Int J Hyg Environ Health. 2017;220:167–78.
107. Den Hond E, Govarts E, Willems H, et al. First steps toward harmonized human biomonitoring in Europe: demonstration project to perform human biomonitoring on a European scale. Environ Health Perspect. 2015;123:255–63.
108. Choi J, Knudsen LE, Mizrak S, Joas A. Identification of exposure to environmental chemicals in children and older adults using human biomonitoring data sorted by age: results from a literature review. Int J Hyg Environ Health. 2017;220:282–98.

109. Koch HM, Rüther M, Schütze A, Conrad A, Pälmke C, Apel P, Brüning T, Kolossa-Gehring M. Phthalate metabolites in 24-h urine samples of the German Environmental Specimen Bank (ESB) from 1988 to 2015 and a comparison with US NHANES data from 1999 to 2012. Int J Hyg Environ Health. 2017;220:130–41.
110. Kolossa-Gehring M, Becker K, Conrad A, Schröter-Kermani C, Schulz C, Seiwert M. Environmental surveys, specimen bank and health related environmental monitoring in Germany. Int J Hyg Environ Health. 2012;215:120–6.
111. Taylor A, Day MP, Marshall J, Patriarca M, White M. Atomic spectrometry update. Clinical and biological materials, foods and beverages. J Anal At Spectrom. 2012;27:537.
112. Hywel Evans E, Palmer CD, Smith CMM. Atomic spectrometry update. Advances in atomic spectrometry and related techniques. J Anal At Spectrom. 2012;27:909.
113. Baglan N, Cossonnet C, Ritt J. Determination of 232Th in urine by ICP-MS for individual monitoring purposes. Health Phys. 2001;81:76–81.
114. McPartland M, Noori B, Garbus S-E, Lierhagen S, Sonne C, Krøkje Å. Circulating trace elements: comparison between early and late incubation in common eiders (Somateria mollissima) in the central Baltic Sea. Environ Res. 2020;191:110120.
115. Thomas R. Practical Guide to ICP-MS. Boca Raton: CRC Press; 2013.
116. Balcaen L, Bolea-Fernandez E, Resano M, Vanhaecke F. Inductively coupled plasma – Tandem mass spectrometry (ICP-MS/MS): A powerful and universal tool for the interference-free determination of (ultra)trace elements – A tutorial review. Anal Chim Acta. 2015;894:7–19.
117. Fernández SD, Sugishama N, Encinar JR, Sanz-Medel A. Triple quad ICPMS (ICPQQQ) as a new tool for absolute quantitative proteomics and phosphoproteomics. Anal Chem. 2012;84:5851–7.
118. Guilhaus M. Essential elements of time-of-flight mass spectrometry in combination with the inductively coupled plasma ion source. Spectrochim Acta Part B At Spectrosc. 2000;55:1511–25.
119. Limbeck A, Galler P, Bonta M, Bauer G, Nischkauer W, Vanhaecke F. Recent advances in quantitative LA-ICP-MS analysis: challenges and solutions in the life sciences and environmental chemistry. Anal Bioanal Chem. 2015;407:6593–617.
120. Vanhoof C, Bacon JR, Fittschen UEA, Vincze L. 2023 atomic spectrometry update – a review of advances in X-ray fluorescence spectrometry and its special applications. J Anal At Spectrom. 2023;38:1730–43.
121. Brouwer P. Theory of XRF. Almelo: PANalytical BV; 2006.
122. Bauer LJ, Mustafa HA, Zaslansky P, Mantouvalou I. Chemical mapping of teeth in 2D and 3D: X-ray fluorescence reveals hidden details in dentine surrounding fillings. Acta Biomater. 2020;109:142–52.
123. Byers HL, McHenry LJ, Grundl TJ. XRF techniques to quantify heavy metals in vegetables at low detection limits. Food Chem X. 2019;1:100001.
124. Zhang Y, Sakurai K. Inter-correlation of impurity trace elements in bloodstone rock: X-ray fluorescence mapping studies. J Anal At Spectrom. 2009;24:1579.
125. Rawat K, Sharma N, Singh VK. X-Ray Fluorescence and comparison with other analytical methods (AAS, ICP-AES, LA-ICP-MS, IC, LIBS, SEM-EDS, and XRD). In: X-Ray fluorescence in biological sciences. Wiley, 2022. pp. 1–20.
126. https://www.epa.gov/amtic/standard-operating-procedures-analysis-chemical-speciation-network-csn-samples-using-x-ray EPA. Accessed 26 Mar 2024.
127. Uo M, Wada T, Sugiyama T. Applications of X-ray fluorescence analysis (XRF) to dental and medical specimens. Jpn Dent Sci Rev. 2015;51:2–9.
128. Geraki K, Farquharson MJ, Bradley DA. Concentrations of Fe, Cu and Zn in breast tissue: a synchrotron XRF study. Phys Med Biol. 2002;47:310.
129. Webb AN, Antipova O, Shughoury S, Farfel JM, Bennett DA, Du Y, Zheng W, Nie LH. Mercury and selenium distribution in human brain tissue using synchrotron micro-X-ray fluorescence. Metallomics. 2024. https://doi.org/10.1093/mtomcs/mfae018
130. Schreiver I, Hesse B, Seim C, et al. Synchrotron-based ν-XRF mapping and μ-FTIR microscopy enable to look into the fate and effects of tattoo pigments in human skin. Sci Rep. 2017;7:11395.
131. XGT-9000. X-ray analytical microscope user manual. Horiba Ltd, Kyoto, 2022.
132. Kihara Y, Makino Y, Yokoyama M, Chiba F, Tanaka A, Nakayama SMM, Hayama S, Ishizuka M, Nolte KB, Iwase H. X-ray analytic microscopy with CT-guided sample extraction to analyze potential projectile fragments in a dead serow. Leg Med. 2023;63:102257.
133. Misra NL. Characterization of nuclear materials by total reflection X-ray fluorescence spectrometry. J Radioanal Nucl Chem. 2014;300:137–45.
134. Gruber A, Müller R, Wagner A, Colucci S, Spasić MV, Leopold K. Total reflection X-ray fluorescence spectrometry for trace determination of iron and some additional elements in biological samples. Anal Bioanal Chem. 2020;412:6419–29.
135. Kunimura S, Kawai J. Portable total reflection X-ray fluorescence spectrometer for Nanogram Cr detection limit. Anal Chem. 2007;79:2593–5.
136. Antosz FJ, Xiang Y, Diaz AR, Jensen AJ. The use of total reflectance X-ray fluorescence (TXRF) for the determination of metals in the pharmaceutical industry. J Pharm Biomed Anal. 2012;62:17–22.
137. Cheung TW, Law AWL, Ahmed R, Mak CY, Lau C. Assessment of bone calcium and phosphorus content using micro X-ray fluorescence spectrometry (μ-EDXRF): effects of long-term cadmium poisoning. X-Ray Spectrom. 2016;45:339–43.
138. Estevam M, Appoloni CR. Use of portable X-ray Fluorescence (PXRF) In Vivo as an alternative technique for the assessment of iron levels in patients with Thalassemia and Hemochromatosis. Health Phys. 2013;104:132–8.
139. Dao E, Zeller MP, Wainman BC, Farquharson MJ. Feasibility of the use of a handheld XRF analyzer to measure skin iron to monitor iron levels in critical organs. J Trace Elem Med Biol. 2018;50:305–11.
140. Izumoto Y, Matsuyama T, Mizuhira M, Imaseki H, Hamano T, Sakai Y, Oguri Y, Yoshii H. Rapid detection of heavy elements in blood extracted from wounds using x-ray fluorescence analysis. J Radiol Prot. 2018;38:1384–92.
141. Buddhachat K, Klinhom S, Siengdee P, Brown JL, Nomsiri R, Kaewmong P, Thitaram C, Mahakkanukrauh P, Nganvongpanit K. Elemental analysis of bone, teeth, horn and antler in different animal species using non-invasive handheld X-Ray Fluorescence. PLoS ONE. 2016;11:e0155458.
142. He L, Lu Y, Li C, et al. Non-targeted metallomics through synchrotron radiation X-ray fluorescence with machine learning for cancer screening using blood samples. Talanta. 2022;245:123486.
143. Specht AJ, Kponee K, Nkpaa KW, Balcom PH, Weuve J, Nie LH, Weisskopf MG. Validation of x-ray fluorescence measurements of metals in toenail clippings against inductively coupled plasma mass spectrometry in a Nigerian population. Physiol Meas. 2018;39:085007.

144. McIver DJ, VanLeeuwen JA, Knafla AL, Campbell JA, Alexander KM, Gherase MR, Guernsey JR, Fleming DEB. Evaluation of a novel portable x-ray fluorescence screening tool for detection of arsenic exposure. Physiol Meas. 2015;36:2443–59.
145. Fleming DEB, Crook SL, Evans CT, et al. Portable X-ray fluorescence of zinc applied to human toenail clippings. J Trace Elem Med Biol. 2020;62:126603.
146. Fleming DEB, Crook SL, Evans CT, et al. Assessing arsenic in human toenail clippings using portable X-ray fluorescence. Appl Radiat Isot. 2021;167:109491.
147. Fleming DEB, Bennett SR, Frederickson CJ. Feasibility of measuring zinc in human nails using portable x-ray fluorescence. J Trace Elem Med Biol. 2018;50:609–14.
148. Fleming DEB, Nader MN, Foran KA, Groskopf C, Reno MC, Ware CS, Tehrani M, Guimarães D, Parsons PJ. Assessing arsenic and selenium in a single nail clipping using portable X-ray fluorescence. Appl Radiat Isot. 2017;120:1–6.
149. Fleming DEB, Kaiser MG, Rankin BD, Schenkels KMM. Assessment of X-ray fluorescence capabilities for nail and hair matrices through zinc measurement in keratin reference materials. J Trace Elem Med Biol. 2023;77:127136.
150. Pitakarnnop T, Buddhachat K, Pakdeenarong P, Nganvongpanit K. Elemental Distribution in Animal Carpal and Tarsal Bones Using Differences in X-ray Fluorescence Energy. Biol Trace Elem Res. 2021;199:874–87.
151. Nguyen J, Crawford D, Howarth D, Sukhu B, Pejović-Milić A, Gräfe JL. Ex vivo quantification of lanthanum and gadolinium in post-mortem human tibiae with estimated barium and iodine concentrations using K x-ray fluorescence. Physiol Meas. 2019;40:085006.
152. Hampton JO, Lohr MT, Specht AJ, Nzabanita D, Hufschmid J, Berger L, McGinnis K, Melville J, Bennett E, Pay JM. Lead exposure of mainland Australia's top avian predator. Environ Pollut. 2023;332:122004.
153. Specht AJ, Steadman DW, Davis M, Bartell SM, Weisskopf MG. Bone lead variability in bone repository skeletal samples measured with portable x-ray fluorescence. Sci Total Environ. 2023;880:163197.
154. Xu Q, Xia W, Zhou L, et al. Determination of hepatic iron deposition in drug-induced liver fibrosis in Rats by confocal Micro-XRF Spectrometry. ACS Omega. 2022;7:3738–45.
155. Turyanskaya A, Rauwolf M, Pichler V, et al. Detection and imaging of gadolinium accumulation in human bone tissue by micro- and submicro-XRF. Sci Rep. 2020;10:6301.
156. Salles S, Salles R, Pavão MSG, Cardoso SC, Stelling MP. Elemental profiles in distant tissues during tumor progression. BMC Cancer. 2023;23:322.
157. Ghanbari Birgani M, Reiazi R, Afkhami Ardekani M, Ghaffari H, Shakeri-Zadeh A, Mofid B. Analysis of trace elements in human hair through X-ray fluorescence spectroscopy for screening of prostate cancer. Med J Islam Repub Iran. 2020;34:86.
158. Webb AN, Spiers KM, Falkenberg G, Gu H, Dwibhashyam SS, Du Y, Zheng W, Nie LH. Distribution of Pb and Se in mouse brain following subchronic Pb exposure by using synchrotron X-ray fluorescence. Neurotoxicology. 2022;88:106–15.
159. Čargonja M, Mekterović D, Žurga P, Ravlić-Gulan J, Radović IB, Žauhar G. Deposition of heavy metals in biological tissues of workers in metal workshops. Environ Sci Pollut Res. 2022;30:36794–806.
160. Zhao K, Li S, Yi P, Guo Y, Yu Q, Zhu C, Feng Q, Du J, Zhang X, Feng Y. Detection of gadolinium deposition in cortical bone with ultrashort echo time T1 mapping: an ex vivo study in a rabbit model. Eur Radiol. 2021;31:1569–77.
161. Chudzińska M, Komorowicz I, Hanć A, Gołdyn R, Barałkiewicz D. Chemometric approach to evaluate element distribution in muscle, liver and fish bone of roach (Rutilus rutilus), silver bream (Blicca bjoerkna) and crucian carp (Carassius carassius) from Swarzędzkie Lake (Poland) using ICP-MS and FIAS-CVAAS techniques. J Environ Sci Health B. 2016;51:790–800.
162. Vuoti E, Palosaari S, Peräniemi S, Tervahauta A, Kokki H, Kokki M, Tuukkanen J, Lehenkari P. In utero deposition of trace elements and metals in tissues. J Trace Elem Med Biol. 2022;73:127042.
163. Christensen JR, LaBine GO, Cheung JS, Rosol R, Mohapatra AK, Laird B, Chan HM. Micro-distribution of arsenic in toenail clippings using laser ablation inductively coupled plasma mass spectrometry: implications for biomonitoring. Environ Monit Assess. 2024;196:181.
164. Rodrigues Gonçalves M, Nogueira Cruvinel VR, Verpaele S, Bashash M, Pintas Marques C, Urbano MR, Paoliello MMB, Aschner M, da Silva SV. Metal levels in waste pickers in Brasilia, Brazil: hair and nail as exposure matrices. J Toxicol Environ Health A. 2024;87:77–90.
165. Andrew AS, O'Brien KM, Jackson BP, Sandler DP, Kaye WE, Wagner L, Stommel EW, Horton DK, Mehta P, Weinberg CR. Keratinous biomarker of mercury exposure associated with amyotrophic lateral sclerosis risk in a nationwide U.S. study. Amyotroph Lateral Scler Frontotemporal Degener. 2020;21:420–7.
166. Hood KM, Sweeney E, Ilie G, Keltie E, Kim JS. Toenail arsenic species and metallome profiles associated with breast, cervical, prostate, and skin cancer prevalence in the Atlantic Partnership for Tomorrow's Health cohort. Front Public Health. 2023. https://doi.org/10.3389/fpubh.2023.1148283.
167. Mehta SQ, Behl S, Day PL, et al. Evaluation of Zn, Cu, and Se levels in the North American Autism spectrum disorder population. Front Mol Neurosci. 2021. https://doi.org/10.3389/fnmol.2021.665686.
168. Arbova DL, Tolmachev SY, Brockman JD. A multi-collector ICP-MS method for quantification of plutonium, uranium, and americium in hair and nails of occupationally or medically exposed individuals. Talanta. 2024;270:125607.
169. Li Y, Meng F, Chen Z, et al. Pharmacokinetics and tissue distribution in rats of a novel anticancer platinum compound LLC-1903. Xenobiotica. 2020;50:980–7.
170. Türkoğlu S, Kaya G. Biomonitoring of toxic and essential trace elements in different tissues of fish species in Türkiye. Food Addit Contam Part B. 2023;16:332–9.
171. Rusch P, Hirner AV, Schmitz O, Kimmig R, Hoffmann O, Diel M. Zinc distribution within breast cancer tissue of different intrinsic subtypes. Arch Gynecol Obstet. 2021;303:195–205.
172. Metarapi D, Schweikert A, Jerše A, Schaier M, van Elteren JT, Koellensperger G, Theiner S, Šala M. Semiquantitative analysis for high-speed mapping applications of biological samples using LA-ICP-TOFMS. Anal Chem. 2023;95:7804–12.
173. Stojsavljević A, Rovčanin B, Jagodić J, Radojković DD, Paunović I, Gavrović-Jankulović M, Manojlović D. Significance of arsenic and lead in Hashimoto's thyroiditis demonstrated on thyroid tissue, blood, and urine samples. Environ Res. 2020;186:109538.
174. Stojsavljević A, Rovčanin B, Krstić Đ, Borković-Mitić S, Paunović I, Kodranov I, Gavrović-Jankulović M, Manojlović D. Evaluation of trace metals in thyroid tissues: Comparative analysis with benign and malignant thyroid diseases. Ecotoxicol Environ Saf. 2019;183:109479.
175. Aydemir D, Simsek G, Ulusu NN. Dataset of the analyzing trace elements and minerals via ICP-MS: Method validation for the mammalian tissue and serum samples. Data Brief. 2020;29:105218.
176. Jayawardene I, Paradis J-F, Bélisle S, Poddalgoda D, Macey K. Multi-elemental determination of metals, metalloids and rare

earth element concentrations in whole blood from the Canadian Health Measures Survey, 2009–2011. J Trace Elem Med Biol. 2021;68:126830.
177. Nava V, Licata P, Biondi V, Catone G, Gugliandolo E, Pugliese M, Passantino A, Crupi R, Aragona F. Horse whole blood trace elements from different sicily areas: biomonitoring of environmental risk. Biol Trace Elem Res. 2023. https://doi.org/10.1007/s12011-023-03889-5
178. Olowoyo JO, Tshoni UA, Kobyana AS, Lion GN, Mugivhisa LL, Koski L, Wärmländer SKTS, Roos PM. Blood lead concentrations in exposed forecourt attendants and taxi drivers in parts of South Africa. J Trace Elem Med Biol. 2024;81:127348.
179. González-Rubio JM, Domínguez-Morueco N, Pedraza-Díaz S, Cañas Portilla A, Lucena MÁ, Rodriguez A, Castaño A, Esteban-López M. A simple method for direct mercury analysis in dried blood spots (DBS) samples for human biomonitoring studies. Environ Int. 2023;177:107958.
180. Komarova T, McKeating D, Perkins AV, Tinggi U. Trace element analysis in whole blood and plasma for reference levels in a selected Queensland population, Australia. Int J Environ Res Public Health. 2021;18:2652.
181. Specht AJ, Zhang X, Goodman BD, Maher E, Weisskopf MG, Nie LH. A Dosimetry study of portable X-ray Fluorescence in Vivo metal measurements. Health Phys. 2019;116:590–8.
182. Sanyal K, Dhara S, Gumber N, Pai RV. A highly sensitive method for uranium quantification in water samples at ultra-trace level by total reflection X-ray fluorescence, after its direct pre-concentration on the surface of amidoxime functionalized quartz sample supports. Talanta. 2023;254:124129.

Publisher's Note Springer Nature remains neutral with regard to jurisdictional claims in published maps and institutional affiliations.

Springer Nature or its licensor (e.g. a society or other partner) holds exclusive rights to this article under a publishing agreement with the author(s) or other rightsholder(s); author self-archiving of the accepted manuscript version of this article is solely governed by the terms of such publishing agreement and applicable law.